Electrochemical and Ultraviolet/Visible/Infrared Spectroscopic Analysis of Heme *a* and a_3 Redox Reactions in the Cytochrome *c* Oxidase from *Paracoccus denitrificans*: Separation of Heme *a* and a_3 Contributions and Assignment of Vibrational Modes†

Petra Hellwig,‡ Stefan Grzybek,‡ Julia Behr,§ Bernd Ludwig,|| Hartmut Michel,§ and Werner Mäntele*,‡

Institut für Biophysik der Johann-Wolfgang-Goethe-Universität, Theodor-Stern-Kai 7 Haus 74, 60590 Frankfurt am Main, Germany, Abteilung Molekulare Membranbiologie, Max-Planck-Institut für Biophysik, Heinrich-Hoffmann-Strasse 7, 60528 Frankfurt am Main, Germany, and Molekulare Genetik, Institut für Biochemie der Johann-Wolfgang-Goethe-Universität, Marie-Curie-Strasse 9, 60439 Frankfurt am Main, Germany

Received September 22, 1998; Revised Manuscript Received November 16, 1998

ABSTRACT: Cytochrome *c* oxidase from *Paracoccus denitrificans* was studied with a combined electrochemical and ultraviolet/visible/infrared (UV/vis/IR) spectroscopic approach. Global fit analysis of oxidative electrochemical redox titrations was used to separate the spectral contributions coupled to heme *a* and a_3 redox transitions, respectively. Simultaneous adjustment of the midpoint potentials and of the amplitudes for a user-defined number of redox components (here heme *a* and a_3) at all wavelengths in the UV/vis (900−400 nm) and at all wavenumbers in the infrared (1800−1250 cm^{-1}) yielded difference spectra for the number of redox potentials selected. With an assumption of two redox components, two spectra for the redox potential at -0.03 ± 0.01 V and 0.22 ± 0.04 V (quoted vs Ag/AgCl) were obtained. The method used here allows the separation of the heme signals from the electrochemically induced visible difference spectra of native cytochrome *c* oxidase without the addition of any inhibitors. The separated heme *a* and a_3 UV/vis difference spectra essentially correspond to spectra obtained for high/low-spin and 5/6-coordinated heme a/a_3 model compounds presented by Babcock [(1988) in *Biological Applications of Resonance Raman Spectroscopy* (Spiro, T., Ed.) Wiley and Sons, New York]. Single-component Fourier transform infrared (FTIR) difference spectra were calculated for both hemes on the basis of these fits, thus revealing contributions from the reorganization of the polypeptide backbone, from the hemes, and from single amino acids upon electron transfer of the cofactors (heme a/a_3, Cu_A, and Cu_B), as well from coupled processes such as proton transfer. A tentative assignment of heme vibrational modes is presented and the assignment of the signals to the reorganization of the polypeptide backbone and to perturbations of single amino acids, in particular Asp, Glu, Arg, or Tyr, is discussed.

Cytochrome *c* oxidase is the terminal enzyme of the respiratory chain and catalyzes the stepwise reduction of oxygen to water. In the course of this process, electron and proton transfer are efficiently coupled to contribute to the formation of an electrochemical proton gradient which drives ATP synthesis. Four redox-active cofactors are involved in electron transfer: Cu_A acts as electron acceptor from cytochrome *c* and transfers the electrons to heme *a*. Further electron transfer leads to the binuclear center, formed by heme a_3 and Cu_B, where oxygen is bound and reduced. For reviews on cytochrome *c* oxidase see (refs *1*−*3*). The structure of the cytochrome *c* oxidase from *Paracoccus denitrificans* was published in refs *4* and *5* and from beef heart oxidase in refs *6* and *7*. Recently the structure of oxidized and reduced beef heart oxidase was characterized (*8*).

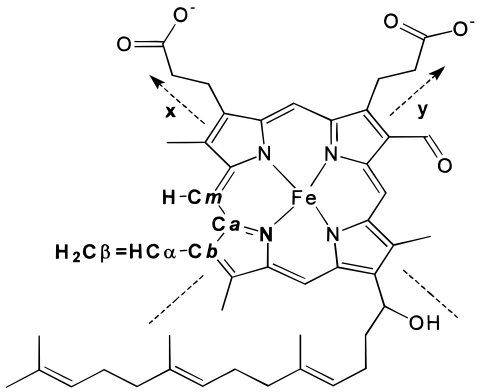

FIGURE 1: Molecular structure of porphyrin *a*. The labeling of the specific C-atoms to describe the vibrations and the pseudosymmetry axes are depicted.

Hemes *a* and a_3 have the same molecular structure (shown in Figure 1) but differ in their spin and coordination state

† Financial support from the Deutsche Forschungsgemeinschaft (Ma 1054/17-1 and 17-2 to W.M., SFB 472 to B.L. and H.M.), the Fonds der Chemischen Industrie (to H.M.) and the Max-Planck-Gesellschaft (to H.M.) is gratefully acknowledged.

* To whom correspondence should be addressed: email maentele@biophysik.uni-frankfurt.de; Tel 49-69-6301-5835; Fax 49-69-6301-5838.

‡ Institut für Biophysik der Johann-Wolfgang-Goethe-Universität.

§ Max-Planck-Institut für Biophysik.

|| Institut für Biochemie der Johann-Wolfgang-Goethe-Universität.

10.1021/bi982282+ CCC: $18.00
Published on Web 01/16/1999

and thus in their electrochemical and spectroscopic properties. Heme *a* has a 6-coordinated low-spin iron center in both oxidation states, and heme a_3 has a 5-coordinated high-spin iron center. UV/vis spectra, in particular in the α-band region (580−610 nm), are characteristic for the heme type and for the redox, coordination, and spin state of the central iron atom (*9*). The optical properties of the two hemes in the cytochrome *c* oxidase have been a source of controversy (*10*−*12*). To separate the optical properties of heme *a* and a_3, heme a_3 was complexed by inhibitors and its redox state thus maintained (*13*). Vanneste (*12*) further developed this method and combined difference absorbance changes deduced upon reduction in the absence and presence of inhibitors and used a photochemically obtained absolute spectrum of the photolabile CO complex of cytochrome a_3^{2+} to determine the spectra for both hemes. This method has been generally accepted since then.

The determination of heme *a* and a_3 redox properties introduced by Horie and Morrison (*13*) and Vanneste (*12*) relies on several assumptions, discussed for example by Hendler and Westerhoff (*14*). One of these assumptions is that heme a_3 is kept in the oxidized state by addition of cyanide, thus allowing added reductants to react exclusively with heme *a*. An additional assumption is that CO can keep heme a_3 in the reduced state and added oxidants react only with heme *a*, and that the addition of charged or uncharged ligands does not affect the optical properties as well as the redox states of the other redox centers. A critical aspect is that spectra from differently prepared enzyme (CO and CN^- inhibited) are used. These prerequisites have been frequently reinvestigated and deserve a closer examination. Sidhu and Hendler (*15*) and Hendler (*16*), for example, presented data indicating that the assumption that CO can keep heme a_3 in the reduced state is not correct. Furthermore, the influence of the inhibition of the binuclear heme−copper center on another redox center could be clearly indicated (*14*, *17*). Liao and Palmer (*18*) have also discussed on the basis of model compound studies and inhibitor-poisoned oxidase discrepancies with Vanneste's data (*12*).

With the method presented here, contributions of the hemes were separated mathematically by globally fitting the redox potential dependency of the absorbance changes and assessing their quantitative contribution. No inhibitors are required and data can be obtained without the need to condition different samples during an oxidative titration. The mathematical analysis allows a clear separation of the individual heme signals. Electrochemical redox titrations in combination with UV/vis spectroscopy were employed to adjust redox states within millivolt precision. This technique, which allows redox reactions to be performed quantitatively and reversibly, was used for stepwise titrations of both hemes, with spectroscopic monitoring in the UV, visible, and IR range.

Published electrochemical properties of the cofactors in the cytochrome *c* oxidase are partly contradictory in both results and interpretation. One of the discussed points is whether the two heme centers have clearly differing midpoint potentials (*10*, *11*, *14*, *19*). In the absence of inhibitors the electron affinity of cytochromes *a* and a_3 is indistinguishable, as described in ref *20*. For the interpretation of the complex data describing the cooperative interactions between the redox centers, several models have been developed. The most prominent one is the neoclassical model (*20*). However, the electrochemical properties of the cytochrome *c* oxidase are still not understood and further studies are required.

The global fit procedure used here has been applied to simultaneously recorded oxidative potential titrations in the IR spectral range. The electrochemically induced Fourier transform infrared (FTIR) difference spectra were correspondingly separated according to the redox potentials of both hemes. The method presented here allows us to distinguish the contributions coupled to electron transfer to/from a certain cofactor, thus introducing the possibility of obtaining more precise assignments in the complex FTIR difference spectra where several difference bands overlap.

MATERIALS AND METHODS

Sample Preparation. Cytochrome *c* oxidase from *P. denitrificans* was prepared as described previously (*4*, *21*). For electrochemistry, cytochrome *c* oxidase solubilized in *n*-decyl β-D-maltopyranoside and 200 mM phosphate buffer (pH 6.9) containing 100 mM KCl, was concentrated to approximately 0.5−1 mM by use of Microcon ultrafiltration cells (Millipore).

Electrochemistry. The ultrathin spectroelectrochemical cell for the UV/vis and IR was used as previously described (*22*, *23*). Sufficient transmission in the entire 1800−1000 cm^{-1} range, even in the region of strong water absorbance at 1645 cm^{-1}, was achieved with the cell path length set to 6−8 μm. The gold grid working electrode was chemically modified by a 2 mM cysteamine solution as reported before (*24*). To accelerate the redox reaction, 16 different mediators were added as reported in ref *24* to a total concentration of 40 μM each. At this concentration, and with the path length below 10 μm, no spectral contributions from the mediators in the visible and IR range could be detected in control experiments with samples lacking the protein, except for the PO modes of the phosphate buffer between 1200 and 1000 cm^{-1}. As a supporting electrolyte, 100 mM KCl was added. Approximately 5−6 μL of the protein solution were sufficient to fill the spectroelectrochemical cell. Potentials quoted with the data refer to the Ag/AgCl/3 M KCl reference electrode; add +208 mV for SHE′ potentials (referring to pH 7).

Spectroscopy. FTIR and UV/vis difference spectra as a function of the applied potential were obtained simultaneously from the same sample with a setup combining an IR beam from the interferometer (modified IFS 25, Bruker) for the 4000−1000 cm^{-1} range and a dispersive spectrophotometer for the 400−900 nm range as reported previously (*23*, *25*). First, the protein was equilibrated with an initial potential at the electrode, and single-beam spectra in the visible and IR range were recorded. A potential step to the final potential was then applied, and single-beam spectra of this state were again recorded after equilibration. Difference spectra as presented here were then calculated from the two single-beam spectra with the initial single-beam spectrum taken as reference. No smoothing or deconvolution procedures were applied. The equilibration process for each applied potential was followed by monitoring the electrode current and by successively recording spectra in the visible range until no further changes were observed. The equilibration generally took less than 10 min under the conditions (protein concentration, electrode modification, mediators)

reported for the full potential step from −0.5 to 0.5 V. Typically, 128 interferograms at 4 cm^{-1} resolution were coadded for each single-beam IR spectrum and Fourier-transformed with triangular apodization.

Redox Titrations. The redox-dependent absorbance changes of the cytochrome *c* oxidase from *P. denitrificans* were studied by performing electrochemical redox titrations in the UV/vis and the IR spectral range. The redox titrations were performed by stepwise setting the potential steps and recording the spectrum after equilibration. Between each potential step, a full potential step was performed. Typically data were recorded at steps of 55 mV. All measurements were performed at 5 °C.

Data Analysis. Both spectroscopy and electrochemistry were controlled by software (MSPEK) developed in our laboratory by D. Moss and S. Grzybek. Data analysis was carried out with two programs developed by S. Grzybek in our laboratory termed EHTIT (*26*) and MEHFIT (*27*).

(A) EHTIT. EHTIT allows to obtain the midpoint potentials E_m and the number *n* of transferred electrons by adjusting a calculated Nernst curve to the measured absorbance change at a single wavelength by an interactive fit. All parameters have to be adjusted manually until the theoretical Nernst curve and the measured data match well (fit by eye).

(B) MEHFIT. The automatic fitting program termed MEHFIT simultaneously adjusts midpoint potentials and amplitudes for a user-defined number of redox components at all wavelengths or wavenumbers of a set of difference spectra (UV/vis or mid-IR) at various redox potentials. In the case presented here, two redox components were fitted (heme a_3 and *a*) and the number of transferred electrons *n* was set to 1 for each component. The linear parts of the Nernst functions—the amplitudes—are fitted by a general linear least-squares routine and the nonlinear parts—the midpoint potentials—are fitted by a Marquardt routine. The sum of squared residuals is minimized by alternating optimization of midpoint potentials and amplitudes. Introduction of weights for each data point offers the possibility to account for the wavelength dependence of the signal-to-noise ratio (at regions of high background absorbance, such as in the IR region around 1650 cm^{-1}, the noise can be significantly higher). Weights were calculated from the standard deviation of 20−40 baseline measurements. The fit yields the midpoint potentials of the predefined number of redox components and their amplitudes at each wavelength. In addition, estimated standard deviations for midpoint potentials and amplitudes and a baseline can be obtained.

RESULTS AND DISCUSSION

UV/vis Redox Titrations. Figure 2 shows an oxidative redox titration of the cytochrome *c* oxidase from *P. denitrificans* in the potential range from −0.2 to +0.4 V in the visible spectral range. The difference spectra thus obtained are termed oxidized-minus-reduced. Positive signals correlate with the oxidized and negative signals with the reduced form of the enzyme. At 445 nm the decrease of the Soret band and at 605 nm of the α-band, respectively, can be seen. Clearly two different potential dependencies of the absorbance changes upon increase of the potential can be observed. Electrochemically induced UV/vis difference spectra for selected potentials have been previously published (*24*).

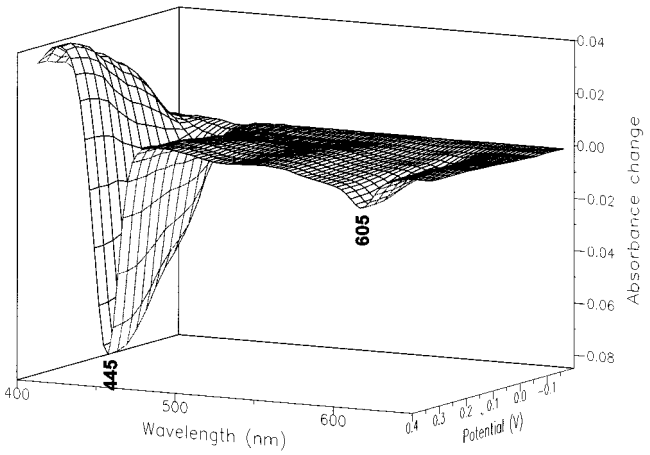

FIGURE 2: Development of the UV/VIS difference spectra (400−700 nm) of the cytochrome *c* oxidase from *P. denitrificans* during an oxidative titration from −0.2 to +0.4 V. For experimental conditions and titration procedure, see Materials and Methods.

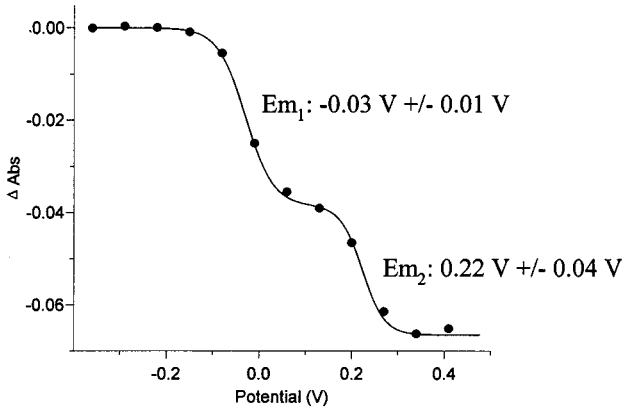

FIGURE 3: Potential dependence of the Soret band at 445 nm in the oxidative redox titration. Solid circles represent the measured data fitted interactively to a calculated Nernst curve (for data analysis see Materials and Methods). Two midpoint potentials can be determined from this fit: E_{m1} at −0.03 V ± 0.01 V and E_{m2} at 0.22 ± 0.04 V. The standard deviation was estimated by comparison of several titrations.

The signals observed in the visible spectral range are assigned to contributions of heme *a* and a_3 (*28*). In addition to these, weaker signals from the Cu_A center can be expected at approximately 480, 530, and 834 nm on the basis of investigations of an isolated subunit II fragment (*29*, *30*). However, these contributions are superimposed by the intense signals from the hemes. Cu_B does not show detectable absorptions in the visible spectral range (*28*).

The potential-dependent development of the Soret band at 445 nm in the oxidative redox titration shown in Figure 2 is presented in Figure 3 (from −0.4 to 0.5 V). The closed circles represent the measured data interactively fitted to a calculated Nernst curve by the program EHTIT (cf. Materials and Methods). Two redox midpoint potentials can be determined from this fit: $E_{m1} = -0.03$ V ± 0.01 V and $E_{m2} = 0.22 \pm 0.04$ V. The error was estimated from the standard deviation of several titrations and is higher for the 0.22 V midpoint potential. This is probably due to the larger number of mediators in the lower potential range (for composition see ref *24*). The close spacing of mediators, approximately all 60 mV, is an important condition for sample equilibration.

We assign the midpoint potential $E_{m1} = -0.03 \pm 0.01$ V to heme a_3 and the midpoint potential $E_{m2} = 0.22 \pm 0.04$ V

to heme *a*. As previously mentioned, there are discrepancies on heme *a* and a_3 electrochemical properties in a number of reports (see for example refs *10*, *11*, *14*, *19*, *31*, and *32*). However, it is generally accepted that the two heme centers do not have clearly distinguishable midpoint potentials, due to their cooperativity and to the cooperativity with Cu_B (*11*, *20*). The titration procedure applied here yielded two clear potential steps. Clear arguments for our assignment are the characteristic optical properties of the two heme centers, differing due to their coordination and spin state and clearly distinguishable in the titration presented here. The potential-dependent absorbance changes observed in the lower potential range show characteristic features (peak position and intensity) of high-spin 5-coordinated heme a_3 model compounds described by ref *28*. The potential-dependent absorbance changes observed in the upper potential range show characteristic features (peak position and intensity) of low-spin 6-coordinated heme *a* model compounds (*28*).

Separation of the Electrochemically Induced Visible Difference Spectra of Hemes a and a_3. The oxidative redox titrations of the difference signals correlated with heme *a* and a_3 redox transitions were separated with a global fit data analysis program developed in our laboratory (MEHFIT, see Materials and Methods). With this program, simultaneous adjustment of the midpoint potentials and of the amplitudes for a user-defined number of redox components (here heme *a* and a_3) at all wavelengths (400−900 nm) for a set of difference spectra taken in the potential range from −0.5 to 0.5 V in steps of 55 mV was performed. The calculation yielded two spectra at midpoint potentials of -0.03 ± 0.01 and 0.22 ± 0.04 V. The method used here enables us to separate the heme contributions from the electrochemically induced visible difference spectra of native cytochrome *c* oxidase without addition of any inhibitors. A separation of the difference signals from the Cu_A center was attempted, but absorbance changes are substantially smaller in relation to the heme signals and a satisfactory separation was not possible.

Figure 4 shows the separated difference spectra calculated for the midpoint potential of heme *a* (spectrum a) and heme a_3 (spectrum b). Figure 4c shows the oxidized-minus-reduced UV/vis difference spectrum for the full potential step from −0.5 to 0.5 V, where the sum of the contributions of heme *a* and a_3 can be observed.

In the oxidized-minus-reduced visible difference spectrum calculated for heme *a* (Figure 4a), the α-band shows a negative signal at 604 nm. The Soret band for the oxidized heme can be seen at 425 nm, and the reduced form absorbs at 444 nm. In the oxidized-minus-reduced visible difference spectrum calculated for heme a_3 (Figure 4b), the Soret band for the oxidized heme can be observed at 414 nm and for the reduced form at 446 nm. The α-band has two minima at 588 and at 609 nm. The absorbance ratio for heme *a* to a_3 is 43:57 (± 8%) at the Soret band from the reduced state at 445 nm, 40:60 (± 8%) of the oxidized form at 417 nm, and for the α-band at 605 nm 68:32 (± 5%). The lower error in the α-band region is due to the higher detector sensitivity (Si photodiode) and lamp intensity (tungsten iodine) in this spectral range.

The UV/vis difference spectrum presented in Figure 4a essentially corresponds to model compound spectra of low-spin 6-coordinated hemes *a* presented in ref *28*, and the difference spectrum in Figure 4b, to model compound spectra of high-spin 5-coordinated hemes *a*. This indicates that the

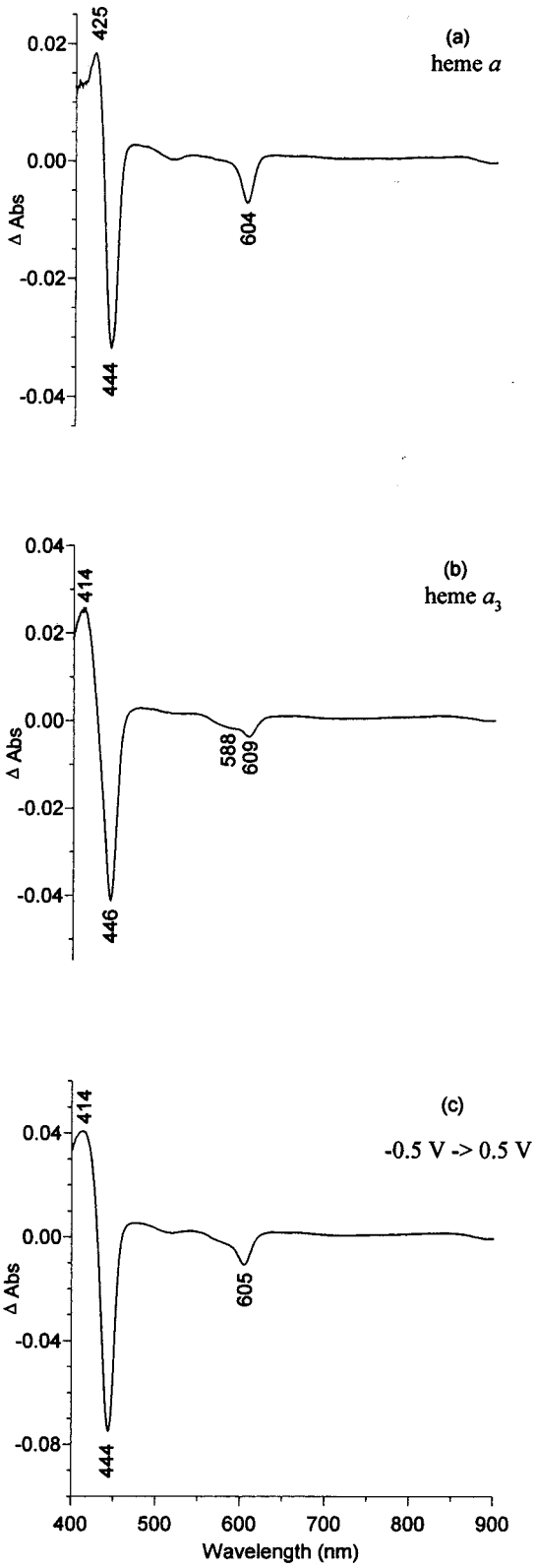

FIGURE 4: Electrochemically induced UV/vis difference spectra of the cytochrome *c* oxidase from *P. denitrificans* calculated for the heme *a* midpoint potential (a) and for the heme a_3 midpoint potential (b) and obtained for the full potential step from −0.5 to 0.5 V (c). Scale for panels a, b, and c differs depending on signal intensity. Positive signals correlate with oxidation and the negative with the reduced form. For experimental conditions and data analysis see Materials and Methods.

spectra calculated for heme *a* and a_3 from the respective midpoint potentials correspond to the spectra of the hemes and that the separation was successful. Discrepancies in the intensity and peak wavelength of the signals can be explained by the differences between the structure of model compounds and heme *a* and a_3 in the protein, as well as by the influence of the protein environment of the hemes.

Clear differences can be observed for the separated heme *a* and a_3 UV/vis difference spectra as compared to the difference spectra that can be obtained by the method introduced by Vanneste (*12*) and described there for the bovine heart oxidase. The most striking discrepancies can be seen in the α-band region. The α-band calculated for heme a_3 absorbs at 609 nm (Figure 4b) and at 603 nm in ref *12*. The position of the α-band in the heme *a* spectrum as well as the position of the Soret bands for both hemes essentially agree with the published values (shifts of $<2-3$ nm); nevertheless, differences in the ratio of band amplitudes are present. These discrepancies can be explained by the influence of subtle differences between the oxidases from different organisms on the optical properties of the hemes. An additional explanation is that the inhibitors (CO, CN^-) used to complex heme a_3 may significantly influence the redox properties and the optical properties of both heme centers.

Separation of the Electrochemically Induced FTIR Difference Spectra of Hemes a and a_3. Figure 5 c shows the oxidized-minus-reduced FTIR difference spectra of the cytochrome *c* oxidase from *P. denitrificans* for the full potential step from −0.5 to 0.5 V. Numerous distinct sharp bands appear throughout the spectrum, with half-widths typically below $5-10$ cm^{-1} (with the exception of the strong difference signal at 1160 and 1088 cm^{-1}). In a previous report, the "forward", i.e., oxidative (−0.5 to +0.5 V), and "reverse", i.e., reductive (+0.5 to −0.5 V), difference spectra were presented for the same enzyme (*33*). These two difference spectra are exact mirror images, thus indicating the full reversibility of the electrochemical redox reaction. The entity of difference signals represent the total of molecular changes concomitant with the redox reactions, i.e., conformational changes of the backbone, from amino acid side chains, protonation processes, and charge redistribution in the cofactor sites, and thus describe the scenario of the enzyme's function. Reversibility is even evident for minute bands such as the signals at $1680-1710$ cm^{-1}. The noise level in these difference spectra can be estimated at frequencies above 1750 cm^{-1}, where no signals appear, and corresponds to approximately $(25-50) \times 10^{-6}$ absorbance units. Only in regions of strong absorbance of the sample, such as around 1650 cm^{-1} (water OH bending mode and amide I C═O mode), is the noise level slightly higher, though never exceeding 10^{-4} absorbance units. These noise levels are confirmed by "blank" difference spectra calculated from two single-beam spectra recorded at the same electrode potential or after a potential cycle (−0.5 to +0.5 V followed by +0.5 to −0.5 V; data not shown). Thus, the "level of confidence" in these difference spectra extends to even very weak bands. Signal contributions in the spectral range from 1800 to 1200 cm^{-1} from mediators and the surface modifier can be excluded because of the choice of experimental conditions, i.e., low concentration of mediators (see Materials and Methods). This statement was confirmed by recording blank difference spectra in samples lacking the protein (data

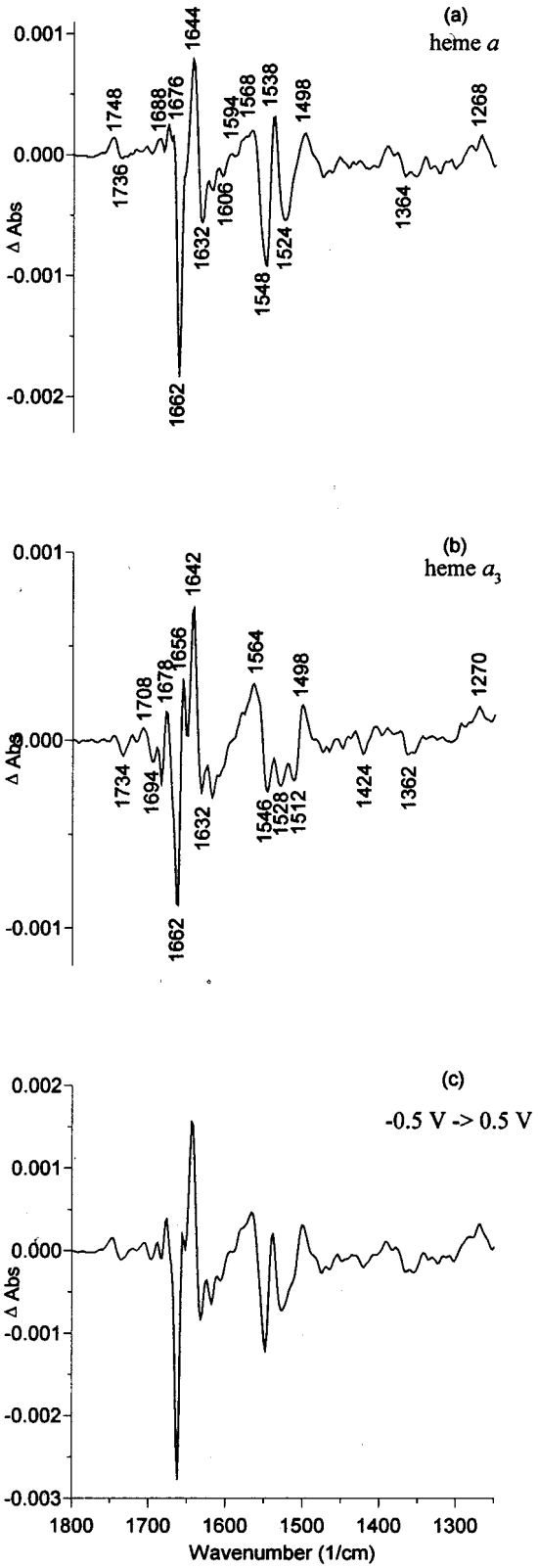

FIGURE 5: Electrochemically induced FTIR difference spectra of the cytochrome *c* oxidase from *P. denitrificans* calculated for the heme *a* midpoint potential (a) and for the heme a_3 midpoint potential (b) and obtained for the full potential step from −0.5 to 0.5 V (c). Scale for panels a, b, and c differs depending on signal intensity. Positive signals correlate with oxidation and the negative with the reduced form. For experimental conditions and data analysis see Materials and Methods.

Table 1: Heme Vibrations[a]

vibration	coupled vibrations	nomenclature	typical spectral range (cm^{-1})
ν(C*a*C*m*)	δ(C*a*C*m*H), δ(C*m*X)	ν_{37}	1560−1625
ν(C*b*C*b*)	ν(C*a*C*m*), ν(NC*a*), ν(C*b*X), δ(C*b*X)	ν_{38}	1535−1570
ν(C*a*C*m*)^{sym}	ν(NC*a*), ν(C*b*C*b*), ν(C*a*C*m*)	ν_{39}	1450−1490
ν(C*a*C*b*)	δ(C*b*X), ν(NC*a*), δ(C*a*C*b*C*b*)	ν_{40}	1435−1450
ν(C*a*N)	ν(C*a*C*b*), δ(C*b*X), δ(C*a*C*b*C*b*)	ν_{41}	1360−1395
δ(C*m*H)	δ(C*b*X), ν(C*a*N), ν(C*a*C*b*)	δ_{42}	1220−1270

[a] The explicit spectral range of the heme modes strongly depends on heme type, redox state and environment. For single references see text.

not shown). The electrochemically induced FTIR difference spectra in Figure 5c are essentially identical to the difference spectra previously reported in refs *24*, *33*, and *34*.

The IR difference spectra presented in Figure 5a,b were calculated on the basis of the midpoint potentials from heme *a* and a_3 presented and discussed above. The oxidative titrations used for the global fits were simultaneously recorded in the UV/vis and IR spectral range, indicating the redox state of the hemes in the electrochemically induced FTIR difference spectra (as described in ref *24*) and the successful separation of the heme signals. We note, however, that spectral contributions due to the reorganization to/from Cu_A and Cu_B upon electron transfer are also involved in these spectra. From their expected midpoint potential (*24*), the involvement in the difference spectrum calculated for heme a_3 potential (Figure 5b) can be assumed.

The comparison of the intensity of the difference signals in Figure 5 spectra a and b shows that the contributions in the spectrum calculated for the heme *a* potential dominate the electrochemically induced FTIR difference spectra for the full potential step presented in Figure 5c. In the case of the dominant difference signal at 1662 cm^{-1}, a major contribution in the spectrum calculated for heme *a* (approximately $^2/_3$ of the total signal amplitude) and a smaller contribution in the spectrum calculated for heme a_3 ($^1/_3$ of the total signal amplitude) can be discerned. Although this might lead to the view that electron transfer from/to heme *a* induces stronger conformational changes than for the corresponding redox process of heme a_3, we favor the view that the redox reactions for both hemes have comparable impact on their protein sites. A final estimation of the molecular reorganization can only be given after a conclusive attribution of the 1662 cm^{-1} band.

The electrochemically induced FTIR difference spectra for the full potential step from −0.5 to 0.5 V and for selected potential steps have been published previously (*24*, *33*). In the approach presented here, the contributions of the hemes can be separated clearly, and tentative assignments of characteristic heme vibrational modes and comparison to resonance Raman data for the same enzyme are possible [see refs *28*, *35*, and *36*]. The nomenclature used in this paper to describe heme modes follows Spiro and Li (*37*) and is summarized in Table 1. The numbering of specific C-atoms to describe the vibrations is shown in Figure 1. For the electrochemically induced FTIR difference spectra, contributions from the porphyrin ring, the formyl groups, the vinyl substituent, and the hydroxyethylfarnesyl side chain can be expected, originating from heme *a* and a_3. Besides the signals of the hemes, the reorganization of the polypeptide backbone and amino acid side chains occurring upon electron transfer of the four redox-active centers heme a/a_3, Cu_A, and Cu_B and coupled processes such as proton transfer can be expected to manifest in the spectra. In the following section the difference spectra calculated for the heme potentials will be described and discussed, and tentative assignments will be presented on the basis of the comparison to IR and Raman spectra of heme model compounds, other oxidases, spectra of isolated amino acids as model compounds, and information on contributions from the secondary structure from infrared absorbance spectra and the deconvolution of the amide I region. These tentative assignments are summarized in Table 2.

A particular problem of the assignment in the difference spectra is the superposition of signals from different constituents of the oxidase, which can lead to the possibility of multicomponent bands and may present ambiguities in the assignment. A spectral region particularly susceptible for overlapping bands is the amide I range. Although in this range (approximately 1690−1610 cm^{-1}) typical contributions from secondary structure elements are expected, and signals may point to alterations of local protein conformation in the course of the redox reaction, we keep in mind that the heme formyl mode also contributes here, as well as specific modes from amino acid side chains. In the following, alternative assignments will thus be discussed along this line whenever applicable.

Assignment of Heme Vibrational Modes: *(A) Porphyrin Ring.* Model compound investigations indicate that the C*a*C*m* vibration (ν_{37}) from the porphyrin ring can be expected between 1586 and 1655 cm^{-1} (*38*). In resonance Raman spectra of the oxidized caa_3 oxidase from *Thermus thermophilus* a signal at 1603 cm^{-1} could be assigned to the ν_{37} vibration of heme *a* and a signal at 1584 cm^{-1} to the ν_{37} vibration of heme a_3 (*36*). Park et al. (*39*) have assigned signals at 1565 and 1580 cm^{-1} to the ν_{37} vibration in photochemically induced FTIR difference spectra of CO-poisoned beef heart oxidase. A direct comparison to these differently obtained spectra and of native and poisoned enzyme must be handled cautiously. In the spectral region where the ν_{37} vibration is expected, several overlapping signals can be observed (Figure 5). The difference bands at 1606 cm^{-1} in the spectrum calculated for heme *a* (Figure 5a) and at 1588 cm^{-1} in the spectrum calculated for heme a_3 (Figure 5b) are possible candidates for an assignment to the ν_{37} vibrational mode.

The C*b*C*b* vibration (ν_{38}) was observed between 1542 and 1604 cm^{-1} in heme *b* model compound studies (*40*). In spectra of type *a* porphyrins, the ν_{38} vibrational mode is expected to split due to the reduced symmetry of the porphyrin ring as compared to type *b* porphyrins (*28*, *35*). The *x* and *y* axes describing the direction of the split vibration (ν_{38x} and ν_{38y}) are introduced in Figure 1. In resonance Raman

Table 2: Tentative Assignments for the IR Spectra Calculated for Heme *a* and a_3 of the Cytochrome *c* Oxidase from *P. denitrificans*

position in heme *a* potential spectrum (cm^{-1})	position in heme a_3 potential spectrum (cm^{-1})	redox state	tentative assignments
1746		ox	Glu 278
1736	1734	red	Glu 278
	1720	ox	ν(C═O) Asp/Glu
	1712	red	ν(C═O) Asp/Glu
	1708	ox	ν(C═O) Asp/Glu
	1694	red	ν(C═O) Asp/Glu
1688		ox	amide I (β-sheet)
	1684	red	amide I (β-sheet)
1676	1678	ox	ν(C═O) CHO heme a_3
			ν(C═O) heme propionates
			$\nu(CN_3H_5)^{as}$ Arg
1662	1662	red	ν(C═O) CHO-heme a_3
			amide I (α-helical)
			$\nu(CN_3H_5)^{as}$ Arg
	1656	ox	amide I (α-helical)
1644	1642	ox	ν(C═O) CHO heme *a*
			amide I (β-sheet)
1632	1632	red	$\nu(CN_3H_5)^{s}$ Arg
			amide I (β-sheet)
1618	1618	red	ν(Cα═Cβ) vinyl group (heme a/a_3)
			amide I (β-sheet)
1606		red	ν(C═O) CHO heme *a*
			ν_{37} heme *a*
			ring O^- Tyr
1594			His
	1588		ν_{37} heme a_3
1580		ox	$\nu(COO^-)^{as}$ Asp/Glu
	1572	ox	$\nu(COO^-)^{as}$ heme propionates
			$\nu(COO^-)^{as}$ Asp/Glu
1568	1564	ox	$\nu(COO^-)^{as}$ heme propionates
			$\nu(COO^-)^{as}$ Asp/Glu
			ring O^- Tyr
			ν_{38x} heme a/a_3
1548	1546	red	ν_{38y} heme *a*
1538		ox	?
	1528	red	$\nu(COO^-)^{as}$ heme propionates
			ν_{38y} heme a_3
1524		red	amide II
	1512	red	ring OH Tyr
1498	1498	ox	ring O^- Tyr
	1424		$\nu(COO^-)^{s}$ Asp/Glu
1380	1380	ox	ν_{41} heme a/a_3
			$\nu(COO^-)^{s}$ heme propionates
1364	1362	red	ν_{41} heme a/a_3
1280		ox	$\nu(CO^-)^{s}$ Tyr
1268	1270	ox	δ_{42} heme a/a_3

spectra of reduced caa_3 oxidase from *T. thermophilus* (*36*) and from aa_3 beef heart oxidase the ν_{38y} vibrational mode could be identified at 1548 cm^{-1} (*35*). In the difference spectrum calculated for heme *a* (Figure 5a) a strong negative signal at 1548 cm^{-1} can be observed. We attribute this signal to the ν_{38y} vibrational mode. The corresponding signal for heme a_3 is assigned to a signal at 1528 cm^{-1} (Figure 5b), on the basis of corresponding resonance Raman data (*35*), which revealed a signal at 1531 cm^{-1}. The ν_{38x} vibrational modes can be expected at 1565−1570 cm^{-1} (*38*). In the difference spectrum calculated for heme *a* (Figure 5a) and for heme a_3 (Figure 5b), difference bands at 1568 cm^{-1} (Figure 5a) and 1564 cm^{-1} (Figure 5b) can be observed and tentatively assigned to this vibration. In the photochemically induced FTIR difference spectra of CO-poisoned beef heart oxidase, the ν_{38} vibrational modes were assigned to signals at 1565, 1540, and 1531 cm^{-1} (*39*); the splitting of the ν_{38} vibrational mode, however, was not discussed.

The absorption of the C*a*N vibration, termed ν_{41}, can be expected between 1319 and 1389 cm^{-1} and could be identified in resonance Raman spectra at 1374 cm^{-1} for the oxidized and at 1365 cm^{-1} for the reduced cytochrome *c* oxidase from *P. denitrificans* (*35*). Park et al. (*39*) proposed difference bands at 1371 and 1366 cm^{-1} for the ν_{41} vibrational modes from photochemically induced FTIR difference spectra of CO-poisoned beef heart oxidase. In the difference spectrum calculated for heme *a* (Figure 5a), a negative signal at 1364 cm^{-1} and a positive signal at 1380 cm^{-1} can be observed. A negative difference band at 1362 cm^{-1} and a positive signal at 1380 cm^{-1} can be observed in the difference spectrum calculated for heme a_3 (Figure 5b). We tentatively assign these signals to the ν_{41} vibrational mode. However, the involvement of the $\nu(COO^-)^s$ from heme propionates has to be considered. These modes were clearly assigned to signals at 1380 cm^{-1} by site specific ^{13}C-labeling of the COOH groups from the heme propionates in the cytochrome *c* oxidase from *P. denitrificans* (*34*). On the basis of the band shape (two maxima/minima can be seen), an involvement of both the ν_{41} vibrational modes and the $\nu(COO^-)^s$ from heme propionates is possible.

The C*m*H vibration (δ_{42}) was observed between 1150 and 1268 cm^{-1} in heme *b* model compound spectra (*40*). The positive signal at 1268 cm^{-1} with a shoulder at 1280 cm^{-1} in the difference spectrum calculated for the heme *a* potential (Figure 5a) and at 1270 cm^{-1} in the difference spectrum calculated for the heme a_3 potential (Figure 5b) can be tentatively assigned to the δ_{42} vibrational mode.

It is clear that, in addition to the modes assigned here, further C−C or C−N vibrations of the porphyrin ring (ν_4, ν_{39}) will contribute to the electrochemically induced FTIR difference spectra. However, we refrain from discussing and assigning these modes on the basis of the data presented here, although bands in the difference spectra are observed in the region where the modes were attributed in Park et al. (*39*) or in resonance Raman spectra. To substantiate these assignments investigations on heme *a* model compounds with the method presented here, as well as ^{13}C-labeling of the hemes, will be necessary.

(B) Formyl Substituent. The C═O bond of the formyl group at the porphyrin ring (for the structure of type *a* porphyrins cf. Figure 1) absorbs between 1680 and 1606 cm^{-1}, depending on hydrogen bonding with neighboring amino acids. The formyl substituent of heme *a* is predicted to form a hydrogen bond to Arg 54, while the same substituent for heme a_3 appears to be free from H-bonding to nearby amino acid residues. On the basis of these structural data (*4*, *5*), different frequencies for the ν(C═O) stretching mode of the formyl group can be expected. In resonance Raman spectra of cytochrome *c* oxidase from *P. denitrificans* and in heme *a* model compounds, a signal at 1610 cm^{-1} could be assigned to the ν(C═O) CHO from reduced heme *a* and at 1649 cm^{-1} to the oxidized form (*28*). For heme a_3, the ν(C═O) CHO of the reduced form could be observed at 1665 cm^{-1} and of the oxidized form at 1674 cm^{-1} (*28*). Park et al. (*39*) discuss signals at 1674 and 1665 cm^{-1} for the ν(C═O) CHO vibration in photochemically induced FTIR difference spectra of CO-poisoned beef heart oxidase. However, the position of the ν(C═O) CHO absorption is

sensitive for ligands such as CO or CN^- (*28*) and a direct comparison to the spectra presented in ref *39* does not appear to be justified.

In the difference spectrum calculated for heme *a* (Figure 5a), the ν(C═O) CHO for the oxidized form can be tentatively assigned to the difference signal at 1644 cm^{-1} and for the reduced form to a signal at 1606 cm^{-1}. We attribute the signals at 1678 cm^{-1} (oxidized form) and 1662 cm^{-1} (reduced form) in Figure 5b to the contributions of the ν(C═O) CHO from heme a_3, strongly supported by resonance Raman data (*28*).

(C) Vinyl Substituent. The ν(Cα═Cβ) vibration of the vinyl substituent was observed at 1620 cm^{-1} for heme *b* model compounds (*40, 41*). Since the influence of the protein site on this vibration is negligible, a comparable absorption can be expected for different heme types and proteins. In resonance Raman spectra of the cytochrome *c* oxidase from *P. denitrificans*, ν(Cα═Cβ) could be observed at 1622 cm^{-1} (*35*). In the difference spectra calculated for the heme *a* and a_3 potential (Figure 5a, b) the ν(Cα═Cβ) vibration can be identified at 1618 cm^{-1}.

(D) Heme Propionates. The contributions of protonated and ionized carboxylic groups of the heme propionates were assigned by specific ^{13}C-labeling of the carboxylic groups of the four heme propionates (*34*). The comparison of the electrochemically induced FTIR difference spectra of wild-type and specific ^{13}C-labeled cytochrome *c* oxidase allowed us to assign a signal at 1676 cm^{-1} to contributions of protonated carboxylic groups. Difference bands at 1570 and 1538 cm^{-1} were assigned to the $\nu(COO^-)^{as}$ vibration and at 1380 cm^{-1} to the $\nu(COO^-)^{s}$ vibration of deprotonated heme propionates. For a detailed discussion cf. ref *34*.

Assignments of Difference Signals to Polypeptide Backbone Modes. In the amide I region (1690−1610 cm^{-1}) a strong negative signal at 1662 cm^{-1} and a positive signal at 1644 cm^{-1} can be observed in the difference spectrum calculated for the heme *a* potential (Figure 5a). At 1632 and 1618 cm^{-1}, negative difference bands and at 1676 cm^{-1} a small positive mode can be seen. In the difference spectrum calculated for the heme a_3 potential, negative signals at 1662, 1632, and 1618 cm^{-1} and positive bands at 1678, 1656, and 1642 cm^{-1} can be observed in the amide I region (Figure 5b).

Amide I signals are predominantly caused by the C═O stretching vibration of the polypeptide backbone. For different secondary structure elements, characteristic absorptions can be distinguished (*42*−*44*). In the electrochemically induced FTIR difference spectra, contributions from the reorganization of the polypeptide backbone upon electron transfer to/from the cofactors can be expected and a partial attribution of the observed signals to amide I modes is conceivable.

The difference signals at 1662 cm^{-1} (Figure 5a,b) are in the range characteristic for the absorbance from α-helical secondary structure elements. The absorbance changes induced by the reorganization of α-helical secondary structure elements are expected to show very small shifts after H/D exchange at most (2−10 cm^{-1}) (*44*). The shift of 1−2 cm^{-1} of this signals after H/D exchange was previously reported in ref *24* and presents an argument for the tentative assignment of the band in the difference spectrum calculated for heme *a* (Figure 5a) to α-helical secondary structure elements. The difference band at 1662 cm^{-1} in Figure 5b could be assigned to the C═O stretching mode of the heme a_3 formyl group in the reduced state as described before, but an additional involvement of amide I modes to this signal should be considered.

Absorptions characteristic for β-sheet secondary structure elements are tentatively attributed to the difference signals at 1644, 1632, and 1618 cm^{-1} (Figure 5a), as well as for the difference signals at 1642, 1632, and 1618 cm^{-1} (Figure 5b). However, conclusive assignments are difficult in this spectral range where difference bands strongly overlap. For the signals at 1688 cm^{-1} (Figure 4a) and 1684 cm^{-1} (Figure 4b), involvement of β-sheet secondary structure elements should thus be considered, too.

In the amide II region (1575−1480 cm^{-1}), strong negative signals at 1548 and 1524 cm^{-1} as well as positive signals at 1568, 1538, and 1498 cm^{-1} can be observed in the difference spectrum calculated for the heme *a* potential (Figure 5a). Negative signals at 1546, 1528, and 1512 cm^{-1} and positive bands at 1564 and 1498 cm^{-1} can be seen in the spectrum calculated for the heme a_3 potential (Figure 5b). Amide II modes result mainly from coupled C−N stretching and N−H bending vibrations. They are much less characteristic for the character of the secondary structure element involved. H/D exchange induces the uncoupling of the C−N and the N−H vibration and shifts the C−N stretching mode to 1490−1460 cm^{-1} and the N−D bending mode to wavenumbers below 1100 cm^{-1}. This implies that the group is accessible to H/D exchange via the solvent. As described previously, an assignment of the signals in the amide II region in the electrochemically induced FTIR difference spectrum of the cytochrome *c* oxidase from *P. denitrificans* appears less probable since little or no shift for H/D exchange was observed (*24*).

Assignments of Amino Acid Side Chains: (A) Aspartate and Glutamate. The C═O group of protonated aspartic and glutamic acid side chains can be expected at wavenumbers higher than 1710 cm^{-1}, depending on their hydrogen bonding. In this spectral region, prominent difference signals at 1746 and 1734 cm^{-1} can be observed (Figure 5c) for the full potential step. These signals were previously reported for the electrochemically induced FTIR difference spectra of the cytochrome *c* oxidase from *P. denitrificans* (*39*) and comprehensively discussed for the fully oxidized potential step as well as for cofactor-specific potential steps (*24*). Difference signals observed for specific potential steps at 1738/1728 cm^{-1} for the potential step from −0.5 to 0.15 V and at 1746/1734 cm^{-1} for the potential step from −0.5 to 0.5 V (*24*) can be compared to the signals in the difference spectra separated from the heme *a* and a_3 midpoint potential (Figure 5a,b) and thus reconfirmed. Electrochemically induced FTIR difference spectra of aspartate and glutamate mutants in the discussed proton pathways (Glu 278, Asp 124, and Asp 399) allowed us to assign clearly Glu 278 to the difference signal at 1746/1734 cm^{-1}. Puustinen et al. (*45*), using a different approach (light-induced difference spectra of CO-poisoned oxidase at 80 K), discuss the involvement of the corresponding amino acid Glu 286 in the bo_3 oxidase from *Escherichia coli* to a difference signal with a comparable absorption.

In the spectrum calculated for the heme a_3 midpoint potential (Figure 5b), difference signals can be seen in the

characteristic spectral region for protonated aspartic and glutamic side chains at 1720/1712 cm^{-1}. These signals can be attributed in a similar way to the protonation/deprotonation of an aspartic or glutamic acid side chain or alternatively to the change of environment for a protonated aspartic or glutamic acid side chain. Since in this spectral region exclusively the absorption of aspartic and glutamic acid side chains is expected, a straightforward assignment is possible.

Investigations on isolated aspartic and glutamic acid side chains show the $\nu(COO^-)^{as}$ stretching mode between 1574 and 1560 cm^{-1} with a higher intensity than the $\nu(C{=}O)$ mode of the protonated forms (*46*). In the respective spectral range, a difference signal at 1580 and 1568 cm^{-1} can be seen in the difference spectrum calculated for the heme *a* midpoint potential (Figure 5a) and at 1572 and 1564 cm^{-1} in the spectrum calculated for the heme a_3 midpoint potential (Figure 5b). Apart from the possible contributions of the deprotonated aspartic and glutamic acid side chains, the involvement of deprotonated heme propionate groups and the ν_{38x} mode described above has to be considered in this complex spectral range with several overlapped bands.

The $\nu(COO^-)^{s}$ stretching mode of ionized aspartic and glutamic acid side chains can be expected at approximately 1404/1420 cm^{-1} with a smaller extinction coefficient than the $\nu(COO^-)$ and the $\nu(C{=}O)$ mode based on investigations on isolated amino acids (*46*). In this spectral region very small difference signals are observed in Figure 5a,b, the difference signal at 1424 cm^{-1} being the most intensive. A clear assignment, however, is not yet possible.

(B) Arginine. Arginine side chains show IR modes at approximately 1673 cm^{-1} [$\nu(CN_3H_5)^{as}$] and 1632 cm^{-1} [$\nu(CN_3H_5)^{s}$], as expected from studies on isolated arginines (*46*). At 1676, 1662, and 1632 cm^{-1} (Figure 5a) and at 1678, 1662, and 1632 cm^{-1} (Figure 5b) difference bands are observed. The involvement of other groups has been discussed before (see Table 2) for these difference bands, and an alternative assignment to arginine side chains cannot be made without further investigations on mutants. There are several arginine side chains in the vicinity of the active centers: Arg 54, Arg 474, and Arg 473. Arg 474 and 473, for example, form ion pairs with the heme propionates and are expected to be involved in electron transfer from Cu_A to heme *a*. Arg 54 has a hydrogen bond to the heme *a* formyl substituent (*4*, *5*). Thus, contributions of Arg side chains in the difference spectra are very likely.

(C) Tyrosine. The ring vibration of protonated tyrosine side chains absorbs at approximately 1516 cm^{-1} and for the deprotonated tyrosine side chain at 1560 and 1498 cm^{-1} (*46*). Another characteristic absorption for deprotonated tyrosine groups can be expected at approximately 1269 cm^{-1} (*46*). In the difference spectrum calculated for the heme *a* midpoint potential (Figure 5a), positive difference bands at 1498, 1564, and 1268 cm^{-1} can be seen. These signals can be attributed to the contribution of a deprotonated tyrosine group that is perturbed upon electron transfer to/from heme *a*. However, structure reveals no deprotonated tyrosine groups and an alternative attribution, i.e., to heme modes, should be considered (*5*). In the spectrum calculated for the heme a_3 midpoint potential shown in Figure 5b, a negative difference band at 1512 cm^{-1} and positive difference bands at 1498, 1564, and 1270 cm^{-1} are observed. A possible interpretation for the observed difference bands is the deprotonation/protonation of a tyrosine group coupled to electron transfer (oxidation/reduction) to/from the binuclear heme−copper center. On the basis of the protein structure (*5*), a critical tyrosine group would be Tyr 280, a group close to the binuclear center. On the other hand, the structure indicated that Tyr 280 has a covalent bonding to His 276 [*5*; for bovine heart oxidase see ref *8*], and uncommon absorptions from this group can be expected due to the reduced symmetry of the ring.

The expected intensity ratio of the ring vibration for the protonated and the deprotonated form (for extinction coefficients see ref *46*) suggests that the signal at 1512 cm^{-1} should be smaller than the signal at 1498 cm^{-1}. On the basis of this comparison, the involvement of a further signal contributing to the 1512 cm^{-1} band can be assumed. In addition to the modes characteristic for tyrosines, the involvement of heme modes has to be considered in this frequency range, too.

In summary, the IR difference spectra presented and discussed here clearly allow spectroscopic signatures of the hemes *a* and a_3 to be separated through redox titrations, without the use of inhibitors to stabilize the redox states. This separation is paralleled by the UV/vis spectra, which clearly document the redox states for each of the hemes. The identification and assignment of the heme modes as well as of modes from individual amino acids presents a step forward in the functional characterization of the metal centers of this enzyme and will be a basis for future IR spectroscopic and electrochemical investigations.

ACKNOWLEDGMENT

We thank Dr. Andreas Barth (Institut für Biophysik, Frankfurt) for extensive literature research on the characteristic absorptions of amino acid side chains. We are grateful to Hannelore Müller for excellent technical assistance.

REFERENCES

1. Ferguson-Miller, S., and Babcock, G. T. (1996) *Chem Rev. 96*, 2889−2907.
2. Babcock, G. T., and Wikström, M. (1992) *Nature 356*, 301−309.
3. Michel, H., Behr, J., Harrenga, A., and Kannt, A. (1998) *Annu. Rev. Biophys. Biomol. Struct. 27*, 329−356.
4. Iwata, S., Ostermeier, C., Ludwig, B., and Michel, H. (1995) *Nature 376*, 660−669.
5. Ostermeier, C., Harrenga, A., Ermler, U., and Michel, H. (1997) *Proc. Natl. Acad. Sci. U.S.A. 94*, 10547−10553.
6. Tsukihara, T., Aoyama, H., Yamashita, E., Tomizaki, T., Yamaguchi, H., Shinzawa-Itoh, K., Nakashima, R., Yaono, R., and Yoshikawa, S. (1995) *Science 269*, 1069−1074.
7. Tsukihara, T., Aoyama, H., Yamashita, E., Tomizaki, T., Yamaguchi, H., Shinzawa-Itoh, K., Nakashima, R., Yaono, R., and Yoshikawa, S. (1996) *Science 272*, 1136−1144.
8. Yoshikawa, S., Shinzawa-Itoh, K., Nakashima, R., Yaono, R., Yamashita, E., Inoue, N., Yao, M., Fei, M. J., Libeu, C. P., Mizushima, T., Yamaguchi, H., Tomizaki, T., and Tsukihara, T. (1998) *Science 280*, 1723−1729.
9. Moore, G. R., and Pettigrew, G. W. (1990) *Cytochromes c*, Springer-Verlag, Berlin and Heidelberg, Germany.
10. Wikström, M. K., Krab, K., and Saraste, M. (1981) *Cytochrome oxidase, A synthesis*, Academic Press, New York.
11. Wikström, M. K. F., Harmon, H. J., Ingledew, W. J., and Chance, B. (1976) *FEBS Lett. 65* (3), 259−277.
12. Vanneste, W. H. (1966) *Biochemistry 5* (3), 838−848.
13. Horie, S., and Morrison, M. (1963) *J. Biol. Chem. 238* (5), 1855−1860.

14. Hendler, R. W., and Westerhoff, H. V. (1992) *Biophys. J. 63*, 1586−1604.
15. Sidhu, G. S., and Hendler, R. W. (1990) *Biophys. J. 57*, 1125−1140.
16. Hendler, R. W. (1991) *J. Bioenerg. Biomembr. 23*, 805−817.
17. Sherman, D., Kotake, S., Ishibe, N., and Copeland, R. A., (1991) *Proc. Natl. Acad. Sci. U.S.A. 88*, 4265−4269.
18. Liao, G.-L., and Palmer, G. (1996) *Biochim. Biophys. Acta 1274*, 109−111.
19. Carter, K., and Palmer, G. (1982) *J. Biol. Chem. 257* (2), 13507−13514.
20. Nicholls, P., and Petersen, L. C. (1972) *Biochim. Biophys. Acta 357*, 462−467.
21. Ostermeier, C., Iwata, S., Ludwig, B., and Michel, H. (1995) *Nat. Struct. Biol. 2*, 842−846.
22. Moss, D. A., Nabedryk, E., Breton, J., and Mäntele, W. (1990) *Eur. J. Biochem. 187*, 565−572.
23. Mäntele, W. (1996) in *Biophysical Techniques in Photosynthesis* (Hoff, A. J., and Amesz, J., Eds.) Chapter 9, pp 137−160, Kluwer, Dordrecht, The Netherlands.
24. Hellwig, P., Behr, J., Ostermeier, C., Richter, O.-M. H., Pfitzner, U., Odenwald, A., Ludwig, B., Michel, H., and Mäntele, W. (1998) *Biochemistry 37*, 7390−7399.
25. Mäntele, W. (1993) *Trends Biochem. Sci. 18*, 197−202.
26. Baymann, F., Moss, D. A., and Mäntele, W. (1991) *Anal. Biochem. 199*, 269−274.
27. Grzybek, S., Baymann, F., Müller, K.-H., and Mäntele, W. (1993) Me_h-Fit: A computer program for the analysis of redox titrations, in *Fifth international conference on the spectroscopy of biological molecules* (Theophanides, T., Anastassopoulou, J., and Fotopoulos, N., Eds.) pp S25−26, Kluwer Academic Publishers, Dordrecht, The Netherlands.
28. Babcock, G. T. (1988) Raman Scattering by Cytochrome Oxidase and by Heme a Model Compounds, in *Biological Applications of Resonance Raman Spectroscopy* (Spiro, T., Ed.) Chapter 7, Wiley and Sons, New York.
29. Lappalainen, P., Aasa, R., Malmström, B. G., and Saraste, M. (1993) *J. Biol. Chem. 268*, 26416−26421.
30. Lappalainen, P., Waltmough, N. J., Greenwood, C., and Saraste, M. (1995) *Biochemistry 34*, 5824−5830.
31. Tiesjema, R. H., Muijsers, A. O., and Van Gelder, B. F. (1973) *Biochim. Biophys. Acta 305*, 19−28.
32. Hendler, R. W., Subba Reddy, K. V., Shrager, R. I., and Caughey W. S. (1986) *Biophys. J. 58*, 897−967.
33. Hellwig, P., Rost, B., Kaiser, U., Ostermeier, C., Michel, H., and Mäntele, W. (1996) *FEBS Lett. 385*, 53−57.
34. Behr, J., Hellwig, P., Mäntele, W., and Michel, H. (1998) *Biochemistry 37*, 7400−7406.
35. Heibel G. E., Hildebrandt, P., Ludwig, B., Steinrücke, P., Soulimane, T., and Buse, B. (1993) *Biochemistry 32*, 10866−10877.
36. Gerscher, S., Hildebrandt, P., Soulimane, T., and Buse, G. (1999) *Biospectroscopy* (in press).
37. Spiro, T. G., and Li, X.-Y (1988) Resonance Raman Spectroscopy of Metalloporphyrins, in *Biological Applications of Resonance Raman Spectroscopy* (Sprio, T., Ed.) Chapter 1, Wiley and Sons, New York.
38. Li, X.-Y, Czernuszewicz, R. S., Kincaid, J. R., Su, Y. O., and Spiro, T. G. (1990) *J. Phys. Chem. 94*, 31−47.
39. Park, S., Pan, L. P., Chan, S. I., and Alben, J. O. (1996) *Biophys. J. 71*, 1036−1047.
40. Berthomieu, C., Boussac, A., Mäntele, W., Breton, J., and Nabedryk, E. (1992) *Biochemistry 31*, 11460−11471.
41. Choi, S., Spiro, T. G., Langry, K. C., Smith, K. M., and La Mar, G. N. (1982) *J. Am. Chem. Soc. 104*, 4345−4357.
42. Krimm, S., and Bandekar, J., (1986) *Adv. Protein Chem. 38*, 181−367.
43. Bandekar, J. (1992) *Biochim. Biophys. Acta 1120*, 123−143.
44. Arrondo, J. L. R., Muga, A., Castresana, J., and Goni, F. M. (1993) *Prog. Biophys. Mol. Biol. 59*, 23−56.
45. Puustinen, A., Bailey, J. A., Dyer, R. B., Mecklenburg, S. L., Wikström, M., and Woodruff, W. H. (1997) *Biochemistry 36*, 13195−13200.
46. Venyaminov, S. Y., and Kalnin, N. N. (1990) *Biopolymers 30*, 1259−1271.

BI982282+